Indocyanine green labeling for optical and photoacoustic imaging of mesenchymal stem cells after in vivo transplantation

(Article begins on next page)

19 August 2024

Journal of Biophotonics

Indocyanine Green labeling for optical and photoacoustic imaging of Mesenchymal Stem Cells after in vivo transplantation.
--Manuscript Draft--

Manuscript Number:	
Full Title:	Indocyanine Green labeling for optical and photoacoustic imaging of Mesenchymal Stem Cells after in vivo transplantation.
Article Type:	Full Article
Section/Category:	
Keywords:	Photoacoustic imaging; Cell tracking; Indocyanine Green; stem cells; Near Infrared Fluorescence Imaging.
Corresponding Author:	Miriam Filippi University of Torino Torino, Torino ITALY
Corresponding Author Secondary Information:	
Corresponding Author's Institution:	University of Torino
Corresponding Author's Secondary Institution:	
First Author:	Miriam Filippi
First Author Secondary Information:	
Order of Authors:	Miriam Filippi
	Francesca Garello
	Francesca Arena
	Chiara Pasquino
	Pierangela Giustetto
	Federica Antico
	Enzo Terreno
Order of Authors Secondary Information:	
Abstract:	The transplantation of Mesenchymal Stem Cells (MSCs) holds great promise for the treatment of a plethora of human diseases, but new non-invasive procedures are needed to monitor the cell fate in vivo. Already largely used in medical diagnostics, the fluorescent dye Indocyanine Green (ICG) is an established dye to track limited numbers of cells by optical imaging, but it can be visualized also by Photoacoustic Imaging (PAI), which provides a higher spatial resolution than pure near infrared fluorescence imaging (NIRF). Because of its successful use in clinical and preclinical examinations, we chose ICG as PAI cell labeling agent. Optimal incubation conditions were defined for an efficient and clinically translatable MSC labeling protocol, such that no cytotoxicity or alterations of the phenotypic profile were observed, and a consistent intracellular uptake of the molecule was achieved. Suspensions of ICG-labeled cells were both optically and optoacoustically detected in vitro, revealing a certain variability in the photoacoustic spectra. Intramuscular engraftments of ICG-labeled MSCs were clearly visualized by both PAI and NIRF over few days after transplantation in the hindlimb of healthy mice, suggesting that the proposed technique retains a considerable potential in the field of transplantation-focused research and therapy.
Additional Information:	
Question	Response
Please submit a plain text version of your	January 14th, 2018

cover letter here.

Please note, if you are submitting a revision of your manuscript, there is an opportunity for you to provide your responses to the reviewers later; please do not add them to the cover letter.

Dear Editor,
we are submitting the manuscript entitled 'Indocyanine Green labeling for optical and photoacoustic imaging of Mesenchymal Stem Cells after in vivo transplantation', that reports on the use of the clinically approved fluorescent dye Indocyanine Green (ICG) as labeling agent for the visualization of Mesenchymal Stem Cells (MSCs) by both Photoacoustic and Fluorescence-based Imaging.
The present study was carried out at multiple levels, ranging from the in vitro characterization of the technique to the in vivo applicative proof. Its novelty and significance can be summarised as follows:
1)The choice of ICG as a safer alternative to conventional photoacoustic nano-sized probes endows the protocol with maximized safety, thus increasing the potential for clinical translatability. The optimal labeling conditions were determined, by identifying the maximum exposure time to the agent that do not alter the viability, proliferation, and marker profile of cells after incubation.
2)In these conditions, a good internalization was obtained, such that efficient optical and photoacoustic imaging of cell suspensions in vitro was feasible, allowing to study the PA spectral properties of ICG.
3)Intramuscular engraftments composed of limited numbers (3.0×105) of labeled MSCs were successfully detected and monitored over time in vivo by both imaging modalities, revealing considerable values of local contrast enhancement in the engraftment site, persisting for days after cell deposition.
4)Even though the Fluorescence-based imaging of several types of ICG-labeled cells was already reported (S. E. Boddington, et al., 2010; V. Sabapathy, et al., 2015), our report shows its fundamental role in integrating the photoacoustic information.
5)The photoacoustic imaging allowed the video recording of the cell deposition into the tissue during the transplantation, as well as the three-dimensional representation of the engraftments, highlighting the potential utility of the technique in facilitating the collection of data with real-time content and the characterization of the cell engraftments.

Successful preclinical studies fuelled an increasing interest for therapeutic interventions based on the transplantation of stem and progenitor cells, capable of stimulating repair and regeneration of damaged tissue in several diseases affecting the cardiovascular, central nervous, and musculoskeletal system. As the photoacoustic imaging could provide good endogenous contrast among soft tissues and improved spatial resolution with respect to pure optical detection of ICG, in our opinion this efficient, safe and simple labeling technique retains a considerable potential in the field of transplantation-focused research and therapy, possibly being relevant for the future development of new strategies for the cell fate surveillance. As such, we believe this contribution may be of interest to a broader readership.

Yours sincerely,
Enzo Terreno

Indocyanine Green labeling for optical and photoacoustic imaging of Mesenchymal Stem Cells after in vivo transplantation.

Filippi M. [1#] and Garello F.[1#], Arena F.[1], Pasquino C.[2], Giustetto P.[1], Antico F. [2], Terreno E.[1]*
 # These authors contributed equally to this work

[1] Molecular and Preclinical Imaging Centers, Department of Molecular Biotechnology and Health Sciences, University of Turin, Via Nizza 52, 10126 Torino, Italy.
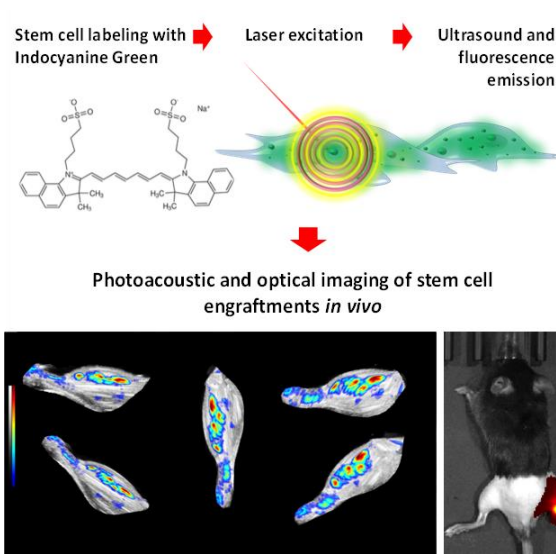
[2] Department of Molecular Biotechnology and Health Sciences, University of Turin, Via Nizza 52, 10126 Torino, Italy.

The transplantation of Mesenchymal Stem Cells (MSCs) holds great promise for the treatment of a plethora of human diseases, but new non-invasive procedures are needed to monitor the cell fate *in vivo*. Already largely used in medical diagnostics, the fluorescent dye Indocyanine Green (ICG) is an established dye to track limited numbers of cells by optical imaging, but it can be visualized also by Photoacoustic Imaging (PAI), which provides a higher spatial resolution than pure near infrared fluorescence imaging (NIRF). Because of its successful use in clinical and preclinical examinations, we chose ICG as PAI cell labeling agent. Optimal incubation conditions were defined for an efficient and clinically translatable MSC labeling protocol, such that no cytotoxicity or alterations of the phenotypic profile were observed, and a consistent intracellular uptake of the molecule was achieved. Suspensions of ICG-labeled cells were both optically and optoacoustically detected *in vitro*, revealing a certain variability in the photoacoustic spectra acquired by varying the excitation wavelength from 680 to 970 nm. Intramuscular engraftments of ICG-labeled MSCs were clearly visualized by both PAI and NIRF over few days after transplantation in the hindlimb of healthy mice, suggesting that the proposed technique retains a considerable potential in the field of transplantation-focused research and therapy.

Stem cells were labeled with the FDA approved fluorescent dye Indocyanine Green (ICG), and detected by both photoacoustic and optical imaging, enabling to monitor the cell fate safely, in dual modality, and with good sensitivity and improved spatial resolution.

1. Introduction

Cell transplantation is an essential tool for biomedical research and a promising approach to achieve curative benefits in several pathologic scenarios.[1] Specifically, due to their major role in regenerative therapies, treatment of immune disorders, and tissue repair, Mesenchymal Stem Cells (MSCs) are commonly involved in cell transplantation-based applications.[1-3] However, these strategies are not regarded as a first-line therapy yet, mainly because of the limited efficacy shown in several clinical studies.[1,4-5] Since the poor results are very often related to the lack of available information about the cell destiny after transplantation,[4-5] a growing interest has been dedicated to the development of innovative imaging procedures for non-invasive surveillance of the cell fate *in vivo*.[5-6] When the transplantation is performed into superficial tissues, also the imaging techiniques with limited penetration depth can be

* Corresponding author: e-mail: enzo.terreno@unito.it, Phone: +39-0116706452, Fax: +39-0116706478

successfully employed to monitor the cell engraftment and the local biological reaction to the therapy.[7-11] Both Optical Imaging (OI) and Ultrasonic Imaging (US) suffer from wave scattering into living tissue, but display other complementary properties.[12-13] Near Infrared Fluorescence (NIRF) imaging is one of the most used OI modalities and it is endowed with elevated sensitivity, but lacks spatial resolution. On the other side, US imaging provides a satisfactory sub-mm spatial resolution at centimeters depth and intermediate sensitivity.[14] Photoacoustic Imaging (PAI) merges the advantages of the two techniques and compensates their limitations, thus paving the way towards new imaging applicative horizons.[12-13] So far, PA cell imaging has been mostly performed by loading cells with gold and carbon-based nano-objects,[15-18] offering a considerable efficiency in contrast detection, but with documented episodes of cytotoxicity and adverse immune reactions.[16,19-20] However, also small molecules (either fluorescence quenchers or low quantum-yield emitters) display properties of interaction with the electromagnetic radiation leading to phototermal conversion and ultrasonic emission.[21] Among fluorescent compounds, we chose Indocyanine Green dye (ICG), a tricarbocyanine dye that, when dissolved in aqueous solution in the micromolar range, exhibits absorbance and emission peaks at 780 nm and 830 nm, respectively.[22-23] Since its FDA approval for human use in 1959,[22] this molecule has been clinically employed for a myriad of medical purposes, including phototherapy, ophthalmic angiography, laparoscopy, hepatic function and cardiac output determination, sentinel lymph node detection in oncology, vascular and brain surgery, and several others.[22-27] With a fluorescence quantum yield of about 10% in water, ICG can non-radiatively release $\approx$ 90% of its excited energy in the form of heat,[28] thus becoming a popular option for the surface functionalization of particles detectable by both NIRF and PAI.[15,21] ICG has already been proposed as cell labeling agent in cell tracking by NIRF,[29-30] but it has never been envisaged for the photoacoustic cell visualization in its molecular form. Besides retaining superior imaging potential than pure NIRF, PAI of cells loaded with ICG would also offer a safer labeling route than current standard probes. Therefore, in the present study, this dye was selected as dual fluorescence and optoacoustic cell tracer to label murine bone marrow-derived MSCs. After having defined the optimal labeling conditions, the characteristics and persistence of NIRF and PA signals were monitored either in *in vitro* cell suspensions or *in vivo* engraftments obtained by intramuscular transplantation in healthy mice.

2. Experimental

2.1 Animal Care and Use

Eight weeks old female C57BL/6J mice with similar weight (around 20-21 g) were used for the *in vivo* tests. All mice involved in the study were obtained from Charles River Laboratories (Calco, LC, Italy) and maintained in standard housing conditions, with water and standard rodent chow *ad libitum* and 12 h light/dark cycle. Anesthesia was provided by intramuscular injection of a combination of tiletamine/zolazepam (Zoletil 100; Virbac, Milan, Italy) at 20 mg/kg and xylazine (Rompun; Bayer, Milan, Italy) at 5 mg/kg. For information about the histological examination, see the Supporting Information. Each animal group was composed of at least 6 individuals. All procedures were approved by the Italian Ministry of Health.

2.2 Chemicals

All the materials necessary for cell culture were purchased from Lonza (Lonza Sales AG, Verviers, Belgium). The ICG dye was purchased from MP Biomedicals (Santa Ana, CA, USA), whereas all other chemicals from Sigma Chemical Co. (St Louis, MO, USA) and were used as received.

2.3 MSC culture

MSCs were isolated from the bone marrow of male C57BL/6J mice (age: 7-9 weeks, weight: 22-28 g). Briefly, femurs and tibias were excised, and flushed with RPMI w/o Red Phenol supplemented with 10% FBS to harvest the bone marrow cells, which were then cultured into Minimal Essential Medium Eagle Alpha Modification supplemented with penicillin (100 U/ml), streptomycin (100 μg/ml), FBS (10%) and glutamine (2 mM). After 4 days, the MSCs were selected on the basis of their adherence to plastic, before they underwent a magnetic immune cell sorting with Microbeads conjugated to monoclonal rat antimouse/human CD11b antibody (Miltenyi Biotec GmbH, Bergish Gladbach, Germany) at day 10 to further remove CD11b$^+$ granulocytic cells.

2.4 Cell labeling protocol

The ICG-labeling solution was prepared by completely dissolving the dye powder into Dimethyl Sulfoxide (DMSO), before adding the FBS-free culture medium (the v/v of DMSO/medium was 1:6). A final ICG concentration of 0.25 mg/ml was used in all experiments. MSCs were detached from flasks, added with the pre-warmed ICG-labeling solution, and left at 37°C for variable time ranges (ranging from 2 minutes to 6 hours). After labeling, the excess of dye was removed by washing the cells three times with Phosphate Buffered Saline (PBS).

2.5 Cell viability and proliferation rate

Cell viability was estimated by using the Trypan Blue exclusion assay. The reported viability percentage value represents the average ratio between the number of viable

cells N_v and the total number of cells N_{tot} ($N_v/N_{tot} \times 100$). Similarly, for proliferation tests the cells were seeded after labeling and maintained in standard culture conditions for different time ranges (up to 8 days), before being counted. The proliferation ability is expressed as the average ratio between the number of cells at each time point N_t and the number of cells present at the beginning of the experiment N_0 (N_t/N_0).

2.6 Flow cytometry

Cells were resuspended in PBS supplemented with 0.1% BSA and incubated with fluorochrome-conjugated monoclonal antibodies (mAb) for 30 min at 4°C. The following mAbs (final dilution: 1/20) were used: anti-CD29-(PE), anti-CD44-APC, anti-CD11b-FITC, anti-CD90-(PE) (BD Bioscience Pharmingen, San Jose, CA, USA), anti-Sca1-(PE) (Cedarlane, Burlington, Ontario, Canada), and anti-CD105-PE (MACS Miltenyi Biotec, San Diego, CA, USA). The fluorescence was measured using the FACS Calibur flow cytometer equipped with CellQuest software (BD Biosciences).

2.7 Optical absorbance and emission of labeled cells

The cell uptake of ICG was estimated by fluorimetry. Briefly, the labeling incubation was carried on for 60 minutes. After exhaustive washing, cells were counted, suspended at the final concentration of 3.0×10^6 cells/ml in PBS, sonicated by using a Bandelin Sonoplus Sonicator (20kHz, 20 W, 30s), and analysed by a FluoroMax-4 Spectrofluorometer (Horiba Scientific, Edison New Jersey, USA) equipped with the driving software FluorEssenceTM for Windows. The number of ICG molecules internalized by the single cell was estimated on the basis of the signal intensity values measured at 803 nm and reported on the calibration curves which were previously obtained. The experiment was repeated four times.

2.8 Cell transplantation

Healthy male C57BL/6J mice (weight: 25-28 g, age: 10-12 weeks) were anaesthetized, and their hindlimbs were shaved. After labeling, 3.0×10^5 MSCs were collected, suspended in 100 μL of PBS, and injected into the gastrocnemius muscle of the right hindlimb by using a 1-ml syringe with a 25-G × 5/8-in needle (BD, Franklin Lakes, NJ). Equivalent numbers of control unlabeled cells were transplanted into the left hindlimb.

2.9 Combined ultrasound and photoacoustic (US/PA) imaging

PAI was performed by using a VisualSonics Vevo 2100 LAZR Imaging Station (VisualSonics, Inc., Toronto, Canada) equipped with a LZ250 transducer operating at 21 MHz frequency that incorporates photoacoustic imaging into high-resolution ultrasound imaging. Cell suspensions were loaded onto a custom-made phantom for photoacoustic *in vitro* acquisitions, equipped with stretched plastic capillaries to contain liquid samples, further surrounded by solified agarose gel to provide favourable interface for US propagation. The photoacoustic transducer was set perpendicularly to the capillaries, such that images reproducing their axial sections were acquired. The PA signal intensity was recorded by switching the excitation over the wavelength range included between 680 and 960 nm, and graphed as a spectrum. The normalized photoacoustic spectrum for each sample was obtained by subtracting the contribution of the blank (either PBS or unlabeled cells suspended in PBS) at each wavelength λ, as follows:

$$NPA_{\lambda =} PA\ sample\ _{\lambda} - PA\ ctrl\ _{\lambda}$$

where *NPA* is the normalized photoacoustic signal, *PAsample* and *PActrl* stand for the photoacoustic intensity at each wavelength λ of each *sample* or *ctrl*, respectively. Each experiment was repeated in triplicate.

For *in vivo* imaging, anaesthetized animals were accurately shaved on their hindlimbs. Combined US/PA images were obtained by overlaying photoacoustic intensities on the ultrasound images with user-defined grayscale thresholds. PA intensity values measured on the transplantation site of labeled cells (right hindlimb) were normalized with respect to the signal recorded on the same anatomical region of the left hindlimb after the injection of the control unlabeled cells, as reported in the following formula:

$$PA\ Enh\ = \frac{PA_{right} - PA_{left}}{PA_{left}}$$

where *PAright* and *PAleft* represent the photoacoustic signal measured in the right and left hindlimb at different wavelengths included between 680 and 960 nm, respectively. Spectra recorded before the cell transplantation (Pre-Injection) were provided to show the local endogenous photoacoustic baseline of the muscular tissue. The signal intensity quantification was carried out at fixed excitation wavelength (810 nm).

2.10 Optical imaging

The photon emission from the labeled cells was measured *in vitro* on the Pearl Imager (LI-COR Biosciences, Lincoln, NE) with preset near infrared excitation (710–760 nm) and emission (810–875 nm) pass band filters to evaluate the ICG signal. The *in vivo* studies were carried out on the IVIS Spectrum Whole Animal Imaging System (Perkin Elmer Inc., Waltham, Massachusetts, USA). The animals were irradiated with filter light of wavelength 745 nm, and an image of emission intensity was collected at 840 nm (field of view = 14 cm, fstop = 2, binning = medium, exposure time = auto). As for the photoacoustic experiments, the fluorescence-imaging signal intensity values were measured on the transplantation site of labeled cells (right hindlimb), and normalized with respect

to control unlabeled cells (left hindlimb). The Fluorescence Imaging Enhancement (*FLIenh*) was expressed as:

$$FLI\,Enh = \frac{FLI_{right} - FLI_{left}}{FLI_{left}}$$

where FLI_{right} and FLI_{left} represent the fluorescence intensity measured in the right and left hindlimb, respectively.

2.11 Statistical analysis

All data were presented as Mean Values ± Standard Error of the Mean (MV±SE). Statistical significance was determined by either the unpaired Student *t*-test or the Analysis of the Variance (ANOVA) test, as indicated in each graph. The *p*-values $\leq$ 0.05 and 0.01 were marked as * and **, respectively.

3. Results

3.1 Optimization of the cell labeling procedure

The labeling procedure was performed by detaching and incubating MSCs with ICG-containing medium at 37°C (**Figure 1A**). According to previous studies,[31] a final ICG concentration of 0.25 mg/mL was selected to perform all labeling experiments, and the procedure was optimized by subjecting the MSCs to different incubation times. For the longest incubation times, an inverse proportionality between cell viability and duration of the labeling was observed (**Figure 1B**), with a significant (*t*-test *p*-value $\leq$ 0.01) viability reduction specifically induced by incubations lasting 3 and 6 h (18.9% and 24.3%, respectively). In these conditions, cells also showed impaired proliferation ability (**Figure 1C**): a decreased fraction of viable cells was found at different time points after labeling, culminating at day 8 when the proliferation rate for both the conditions was dramatically reduced (33.3 % and 40.7 %, respectively, ANOVA *p*-value $\leq$ 0.01) with respect to control cells. In the other tested labeling times, no relevant changes in viability were detected, therefore suggesting that an incubation time of 1 h may be considered optimal for safe labeling in maximum loading conditions. The molecular internalization rate after 1h incubation was therefore determined by estimating the ICG content per cell via fluorimetric assay directly on labeled cell suspensions, such that an uptake of $(1.7 \pm 0.4) \times 10^{10}$ molecules/cell was calculated, corresponding to an internalization efficiency of approximately 0.9 ± 0.2 %. Finally, as observed by flow cytometry, the 1 h exposure to ICG did not induce any alteration in the expression profile of cell surface markers

(**Figure 1D**), revealing a complete retention of the MSC phenotype.

3.2 In vitro imaging

The photoacoustic and fluorescent properties of ICG were preliminary investigated with the respective imaging systems (**Figure 2 and 3**). The photoacoustic signal of differently concentrated ICG aqueous solutions in a submillimolar range was acquired by tuning the excitation wavelength from 680 to 970 nm in order to study the PA sensitivity and spectrum *in vitro* (**Figure 2A and B**). The intensity at the initial phase of the spectral profile increased with the dye concentration, and even if a photoacoustic detection limit of 25 μM was identified elsewhere on a different PA imaging station,[32] in our setup we were able to clearly detect the molecule at a concentration of 15 μM (**Figure 2A**) according to what was already reported by others using the same instrument.[33] The PA signal tended to drop as the excitation was swept to high wavelengths (> 830 nm) and became eventually negligible at 950 nm, even at the highest concentration tested (*i.e.*, 1 mM). However, a certain concentration-dependent variability in the spectral shapes was observed: whereas the 1 mM ICG presented a sharp peak centered at 710 nm, in diluted solutions the molecule displayed a more flattened spectral profile characterized by the presence of two peaks. Further lowering the concentration, a more defined peak at 800 nm appeared. Since this observation approximately matched the finding of a recurrent main peak at around 810 nm reported by Park *et al.*[32], we selected this excitation wavelength as reference value to perform the signal quantification and acquire representative images. In order to test the effects of a possible interaction between ICG and cellular components, samples containing the dye at variable concentrations and a fixed number (3.0×10^5) of MSCs were analyzed immediately after mixing (**Figure 2C and D**). Interestingly, in the presence of cells the PA signal intensity at the spectral initial phase increased for almost all the samples (*ca.* 2-fold increase at 15 and 100 μM and even 3-fold at 1 mM ICG). Although some variations in the spectral shape were observed at the highest investigated ICG concentration, for the micromolar ICG the main peak wavelength shifted within the 800-820 nm interval, confirming that the PA excitation may be performed at maximum efficacy in this range. Finally, also cells labeled with the ICG according to our optimized protocol were analyzed (**Figures 2E** and 2**F**). This experiment was carried out by resuspending 3.0×10^5 ICG-labeled MSCs in decreasing PBS volumes, thus varying both the cell density and the final volume of the suspension. We assumed that the ICG amount uptaken by the cells during the labeling procedure led to a final dye

concentration in the μM range, as it was previously determined by fluorimetry. Indeed, the spectral shape of the labeled MSCs recapitulated the one observed in the presence of the micromolar dye, being characterized by a main peak at about 820 nm. Very interestingly, the ICG internalized within cells produced a strong PA signal, which increased of *ca.* 25 % and 85 % as compared to the 100 μM ICG sample with and without cells, respectively. Indeed, the PA signal intensity was comparable to that of the 1 mM ICG mixed with cells (**Figure 2G**), thus indicating that an optoacoustic enhancement can likely be obtained through the intracellular compartimentalization of the dye. Interestingly, only subtle variations in the PA signal intensity were found when labeled cells were differently concentrated into PBS (**Figures 2E and 2F**), possibly suggesting that phenomena of liquid reabsorption that commonly follow the inoculation of cells into tissue might only induce minimal effects on the signal intensity. All the samples were also analyzed in terms of NIRF intensity, as expressed in Average Radiant Efficiency (**Figure 3**). For both ICG aqueous solutions and ICG-cell mix, the concentration-dependent initial increase of the fluorescence peaked at 50 μM, and was followed by a fast decrease (**Figures 3A** and **3B**) in accordance to previous studies indicating that dye concentrations exceeding 200 μM are not detectable due to quenching phenomena.[32] The fluorescent behaviour of ICG only differed at 100 μM, where a slightly reduced emission occurred in the presence of cells. Interestingly, in the suspensions of ICG-labeled cells (**Figures 3C** and **3D**) the NIRF contrast enhancement calculated over the baseline (unlabelled cells) at the lowest and highest cell concentrations (namely 3000 and 15000 cell/μl) corresponded to +300 and 220%, respectively, therefore showing a mild reduction of the fluorescent emission towards high cell densities. Nonetheless, these signal variations were recorded in the same magnitude range of intensity, reflecting a relatively limited potential of the cell density to affect the NIRF emission. Additionally, we also demonstrated that both the photoacoustic and fluorescent emissions increased with the incubation time (**Figure S1A**), but whereas the PA signal amplitudes recorded on suspensions of cells labeled for 2 minutes were not distinguishable from the baseline, the fluorescent signal could be detected in all the tested conditions (**Figure S1B and C**). Finally, the PA and NIRF signal intensity from cells incubated for 1 h was significantly (ANOVA, *p*-value < 0.01) higher with respect to all other conditions (**Figures S1A and S1B**), confirming this incubation time as optimal for imaging efficiency.

3.3 In vivo imaging

The *in vivo* study was carried out by locally transplanting $3.0{\times}10^5$ ICG-labeled MSCs into the gastrocnemius muscle of the right hindlimb of healthy C57BL/6J mice. The site of cell deposition was clearly detected by US imaging (B-mode, 21 MHz), as a consequence of the change in the acoustic impedance determined by the dense inoculated cell mass (**Figure 4A**). The PA signal intensity generated by the ICG-MSCs was normalized over the local endogenous baseline recorded in the left hindlimb of the animal where the transplantation of control unlabeled cells was performed (representative pictures in **Figure 4B**) and expressed as photoacoustic enhancement (PA_{Enh}, see Experimental for details). The PA_{Enh} was measured over the entire range of excitation wavelengths immediately after cell transplantation, then monitored over time, and reported as PA spectrum in **Figure 4C**. Interestingly, immediately and 4 hours post-injection, the maximum peak recorded in the photoacoustic spectra was shifted towards high excitation wavelength values (890 and 920 nm, respectively), whereas from day 1 to day 4, the spectral shape reproduced the one observed *in vitro* with a maximum enhancement centered at around 810 nm (**Figures 4D and 4E**). Finally, the normalized PA spectra acquired 7 days post injection presented a flat shape without any discernable peak. **Figure 4F** displays the time-dependent variation of the signal as quantified at both 810 nm and the wavelength corresponding to the maximum peak recorded in each spectrum, whereas **Figure 4G** shows representative images of the time evolution of PA emission in regions of interest (ROIs) at tissue depth comprised between 1 and 5 mm. Moreover, the entire procedure of cell injection was caught on video (**Movie S1**) and 3D reconstructions of the ICG-MSC engraftment in the right calf were elaborated using Vevo®Lab 1.7.2 software (**Figure S2** and **Movies S2 and S3**). Immediately after cell transplantation, a considerably high PA amplitude was measured in the inoculation site (**Figures 4C and 4F**). By summing up the PA signal areas as calculated on bidimensional ROIs drawn in consecutive images over the entire muscular region, an engraftment volume of around 70 mm^3 was estimated, which is consistent to the injection procedure of a 100 μl cell suspension. Then, a progressive time-dependent decrease in the signal intensity occurred, revealing that the labeled MSCs could be optoacoustically detected until 3 days before the loss of the ICG-related signal and the prevalence of unspecific signal components let the contrast enhancement become almost negligible (**Figure 4F**). After each PA acquisition, the mice underwent NIRF imaging in order to assess the fluorescent contrast enhancement (FLI_{Enh}) produced by the transplanted cells (**Figures 5A** and **5B**). Interestingly, before progressively fading over days (likely due to the dye degradation and washout), the FLI_{Enh} values followed an initial rising trend during the first 24 h after the engraftment deposition. The coincident observation of extremely high PA amplitudes (**Figures 4C and 4F**) suggests that at early time points the strong intermolecular interactions among ICG molecules

contribute to the quenching of the fluorescence, but results at the same time into an increase of the photoacoustic effect, due to photothermal conversion by nonradiative decay.[33] Finally, the time limit for the engraftment detection by NIRF matched that one enabled by the optoacoustic decay (namely, 3 days *p.i.*). Similar conclusions derived from an additional series of experiments perfomed by transplanting a higher cell number (1.0×10^6 cells, **Figures S3 and S4**). As expected, a more intense and persistent contrast enhancement was obtained in both techniques, pushing further the detection limit day. In particular, a photoacoustic signal was still detected 7 days after transplantation, which truly corresponded to sparse residual ICG-labeled MSCs, as proved by histological examination in the inoculation site (**Figure S5**).

4. Discussion

According to pre-clinical and clinical research conducted thus far, cell imaging should be assimilated into more studies focused on the use of cell-transplantation for therapeutic purposes.[30] In fact, the imaging techniques that facilitate the unambiguous *in vivo* identification and characterization of the cell engraftments are invaluable for assessing the survival and the functional integration of exogenous cells, and for optimizing the delivery as well. The present work aimed at addressing these issues by merging the advantages offered by the well-known and safe profile of ICG with the emergent technique of PAI. For the first time the potential application of the free ICG as cell labeling agent and photoacoustic tracer was explored. As already done by Uthaman *et al.*,[34] the PA visualization of the cell engraftment was paralleled by NIRF acquisition in order to perform a comparative study of the two imaging modalities. Despite the minor toxicity and the related advantages for *in vivo* applications, ICG exhibits very complex optical properties. Besides being largely dependent on the solvent, concentration and interaction with other molecules,[22,23,26] the absorption and emission spectra are also broad and overlapping, thus causing a significant re-absorption of the fluorescence by the dye itself. Moreover, as extensively reviewed by Desmettre *et al.*,[22] the molecule can be affected by photodegradation and, at high concentrations, its effective absorption does not linearly increase with concentration due to the dye aggregation. More in details, because of its amphiphilic properties, ICG is mainly present in the monomer form at concentrations below 5 µM, whereas over 100 µM the oligomer form prevails. The ICG oligomers display a weaker fluorescence yield, affecting the absorbance spectrum. Thus, a dramatic boost of the ICG concentration is not expected to result in a substantial signal enhancement, as we also noticed by both PA and NIRF imaging. Alternatively, in order to increase the quantum yield and the fluorescence intensity of the

carbocyanine dye, a stable interaction with phospholipids could be envisaged.[35] Such crucial aspect has been extensively exploited for the preparation of several ICG-loaded nanosystems thus far,[35-36] and coherently, in our experiments the simple mixture of ICG with cells produced a marked increase in the PA intensity values, which could be possibly ascribed also to its interaction with cell membranes. On the other hand, the additional PA increase we observed in the cells after incubation with the dye could be hypothetically justified also by a mechanism of oligomer formation occurring as a consequence of the intracellular compartmentalization. Importantly, in the present study a cell labeling procedure advantageous in terms of both cellular uptake and generated imaging signal was proposed. Remarkably, in these conditions the exposure to the contrast agent did not produce any relevant alteration in the cell profile, suggesting that ICG-labeled MSCs may retain their therapeutic efficacy. Finally, when it comes to *in vivo* use of the ICG, the results interpretation is further complicated by the intricacy of molecular interactions with the various components of the biological environment.[22,34] Here, the photoacoustic behaviour of the dye was investigated in complex circumstances involving concentration-dependent effects, internalization by cells, interactions with cell components, and deposition into living tissues. Since several common applicative scenarios require the transplantation of hundreds of thousands of MSCs,[37-38] we representatively performed our experiments by labeling and monitoring 3.0×10^5 cells to verify whether this procedure could be of effective utility and practical interest. Our *in vivo* proof of principle productively demonstrated that cells can be visualized into living tissue by both PAI and NIRF over few days after transplantation. Though the ICG labeling enables the longitudinal monitoring of the engrafted cells, the observation times are shorter than for the PA-detectable nano-objects reported in literature,[17] most likely due to the faster release of the dye from cells, as already observed by Boddington *et al.*[29] However, also the risks connected to the long-term tissue accumulation of exogenous compounds have to be carefully considered, especially in proximity of delicate therapeutic cell grafts. Additionally, we established that a reliable quantification of the photoacoustic signal at 810 nm can be performed only starting from 24 h after transplantation, since the prior time points are affected by a bathochromic shift of the ICG signal, possibly related to the extremely high local concentration of the dye. As in the same time window we detected the co-presence of PA peaks centred at around 900 nm and reduced NIRF signal, we argued that the two phenomena may be correlated by an exchange of the emission mechanism (*i.e.* from radiative to acoustic), likely depending on the ICG concentration. However, in general terms, it also has to be taken into account that immediately or shortly after surgery, tissues frequently display imaging artefacts caused by haemorrhages and/or micro air bubbles deposition, which make it arduous to

define the real source of the observed contrast, thus preventing an accurate quantification in early monitoring. This aspect becomes more relevant when the local transplantation is carried out in the absence of specific cell vehicles (like hydrogels), such that the injection procedure likely introduces air into tissue along the needle path.[39] Therefore, we conclude that the optimal imaging window offered by the present protocol corresponds to a time range comprised between 1 and 3 days post-transplantation, which could ideally turn out to be helpful in prospective clinical or pre-clinical applications to: (*i*) ascertain the successful outcome of surgical cell deposition, (*ii*) describe the extension and aspect of the engraftment, and (*iii*) follow the cell migration in relatively superficial anatomical areas. Finally, we demonstrated that NIRF imaging substantially recapitulated and validated the information obtained by PAI, thus highlighting the pivotal role of the dual-modality approach in strengthening the reliability and clinical utility of ICG-guided MSC imaging. In the past decade, researchers have been tracking transplanted cells in real-time *in vivo* mainly by Magnetic Resonance Imaging (MRI), Positron emission Tomography (PET), Single Photon Emission Tomography (SPECT), and Optical Imaging, facing crucial issues in regard to image acquisition time, method sensitivity, radiation-related damage, short half-life of radioisotopes, genetic manipulation to introduce reporter genes, and three dimensional anatomical imaging capability.[5-11,39] The high spatial resolution integrated with elevated sensitivity and moderate tissue penetration depth, the FDA-approved tracer and the fast image acquisition make of the herein proposed protocol an attractive option to further develop the techniques of direct stem cell labeling towards the clinical dimension, by satisfying almost all the ideal translational requirements.[40]

5. Conclusion

In summary, the ICG was successfully used as PA-NIRF dual-mode contrast agent to label, visualize, and monitor MSCs both *in vitro* and *in vivo*. Proper cell labeling conditions were selected such that the cell uptake was maximized, and cell viability, proliferation, and phenotypic features were preserved. Since the number of MSCs involved in several experimental circumstances is usually either similar or higher than that used here,[35-36] we conclude that in a forward-looking vision this technique retains a considerable potential for transplantation-focused research and therapy by providing the *in vivo* cell fate surveillance with safety, real time content, good endogenous contrast among soft tissues and improved spatial resolution.

Supporting Information

Additional supporting information may be found in the online version of this article at the publisher's website.

Author biographies please see Supporting Information online.

References

1. E. Buzhor , L. Leshansky, J. Blumenthal, H. Barash, D. Warshawsky, Y. Mazor, and R. Shtrichman, Regen Med **9**, 649-672 (2014).
2. X. Wei, X. Yang, Z. P. Han, F. F. Qu, L. Shao, and Y. F. Shi, Acta Pharmacol Sin **34**, 747-754 (2013).
3. M. Das, I. B. Sundell, and P. S. Koka, J Stem Cells **8**, 1-16 (2013).
4. C. A. Herberts, M. S. Kwa, and H. P. Hermsen, J Transl Med **9**, 29 (2011).
5. A. K. Srivastava and J. W. Bulte, Stem Cell Rev **10**, 127-144 (2014).
6. M. E. Kupfer and B. M. Ogle, Biotechnol J **10**, 1515-1528 (2015).
7. Y. Zhao, A. J. Bower, B. W. Graf, M. D. Boppart, and S. A. Boppart, Methods Mol Biol **1052**, 57-76 (2013).
8. E. J. Sutton, T. D. Henning, B. J. Pichler, C. Bremer, and H. E. Daldrup-Link, Eur Radiol **18**, 2021-2032 (2008).
9. Z. Yang, Q. Zeng, Z. Ma, Y. Wang, and X. Xu, J Vis Exp **31**, 10.3791/1388 (2009).
10. J. E. Kim, S. Kalimuthu, and B. C. Ahn, Nucl Med Mol Imaging **49**, 3-10 (2015).
11. Y. Hakamata, T. Murakami, and E. Kobayashi, Transplantation **81**, 1179-1184 (2006).
12. R. Bouchard, O. Sahin, and S. S. Emelianov, IEEE Trans Ultrason Ferroelectr Freq Control **61**, 450-466 (2014).
13. J. Kim, D. Lee, U. Jung, and C. Kim, Ultrasonography **34**, 88-97 (2015).
14. L. Cunha, I. Horvath, S. Ferreira, J. Lemos, P. Costa, D. Vieira, D. S. Veres, K. Szigeti, T. Summavielle, D. Máthé, and L. F. Metello, Mol Diagn Ther **18**, 153-173 (2014).
15. X. Yang, E. W. Stein, S. Ashkenazi, and L. V. Wang, Wiley Interdiscip Rev Nanomed Nanobiotechnol **1**, 360-368 (2009).
16. S. Manohar, C. Ungureanu, and T. G. Van Leeuwen, Contrast Media Mol Imaging **6**, 389-400 (2011).

17. S. Y. Nam, L. M. Ricles, L. J. Suggs, and S. Y. Emelianov, PLoS One **7(5):e37267**, 10.1371/journal.pone.0037267 (2012).

18. H. Gong, R. Peng, and Z. Liu **65**, 1951-1963 (2013).

19. A. J. Andersen, P. P. Wibroe, and S. M. Moghimi, Adv Drug Deliv Rev **64**, 1700-1705 (2012).

20. Z. Krpetić, S. Anguissola, D. Garry, P. M. Kelly, and K. A. Dawson, Adv Exp Med Biol **811**, 135-156 (2014).

21. S. Zackrisson, S. M. Van de Ven, and S. S. Gambhir, Cancer Res **74**, 979-1004 (2014).

22. T. Desmettre, J. M. Devoisselle, and S. Mordon, Surv Ophthalmol **45**, 15-27 (2000).

23. B. Yuan, N. Chen, and Q. Zhu, J Biomed Opt **9**, 497-503 (2004).

24. J. T. Alander, I. Kaartinen, A. Laakso, T. Pätilä, T. Spillmann, V. V. Tuchin, M. Venermo, and P. Välisuo, Int J Biomed Imaging **2012:940585**, 10.1155/2012/940585 (2012).

25. H. Abe, T. Mori, T. Umeda, M. Tanaka, Y. Kawai, T. Shimizu, H. Cho, Y. Kubota, Y. Kurumi, and T. Tani, Surg Today **41**, 197-202 (2011).

26. C. Jonak, H. Skvara, R. Kunstfeld, F. Trautinger, and J. A. Schmid, PLoS One **6(8):e23972**, 10.1371/journal.pone.0023972 (2011).

27. R. Alford, H. M. Simpson, J. Duberman, G. C. Hill, M. Ogawa, C. Regino, H. Kobayashi, and P. L. Choyke, Mol Imaging **8**, 341-354 (2009).

28. M. Ogawa, N. Kosaka, P. L. Choyke, and H. Kobayashi, Cancer Res **69**, 1268-1272 (2009).

29. S. E. Boddington, T. D. Henning, P. Jha, C. R. Schlieve, L. Mandrussow, D. DeNardo, H. S. Bernstein, C. Ritner, D.

30. Golovko, Y. Lu, S. Zhao, and H. E. Daldrup-Link, Cell Transplant **19**, 55-65 (2010).

30. V. Sabapathy, J. Mentam, P. M. Jacob, and S. Kumar, Stem Cells Int **10.1155:2015**, 10.1155/2015/606415 (2015).

31. J. D. Ho, R. J. Tsai, S. N. Chen, and H. C. Chen, Br J Ophthalmol **88**, 556-559 (2004).

32. S. Park, J. Kim, M. Jeon, J. Song, and C. Kim, Sensors (Basel) **14**, 19660-19668 (2014).

33. G. Ferrauto, F. Carniato, E. Di Gregorio, L. Tei, M. Botta, and S. Aime, Nanoscale **9**, 99-103 (2017).

34. S. Uthaman, J. S. Bom, H. S. Kim, J. V. John, H. S. Bom, S. J. Kim, J. J. Min, I. Kim, and I. K. Park, J Biomed Mater Res B Appl Biomater **104**, 825-34 (2016).

35. J. C. Kraft and R. J. Y. Ho, Biochemistry **53**, 1275-1283 (2014).

36. E. Portnoy, N. Vakruk, A. Bishara, M. Shmuel, S. Magdassi, J. Golenser, and S. Eyal, Theranostics **6**, 167-76 (2016).

37. K. Serigano, D. Sakai, A. Hiyama, F. Tamura, M. Tanaka, and J. Mochida, J Orthop Res **28**, 1267-1275 (2010).

38. K. Mareschi, D. Rustichelli, R. Calabrese, M. Gunetti, F. Sanavio, S. Castiglia, A. Risso, I. Ferrero, C. Tarella, and F. Fagioli, Stem Cells Int **2012:920581**, 10.1155/2012/920581 (2012).

39. E. Bull, S.Y. Madani, R, Sheth, A. Seifalian, M. Green, and A. M. Seifalian, Int J Nanomedicine **9**, 1641-1653 (2014).

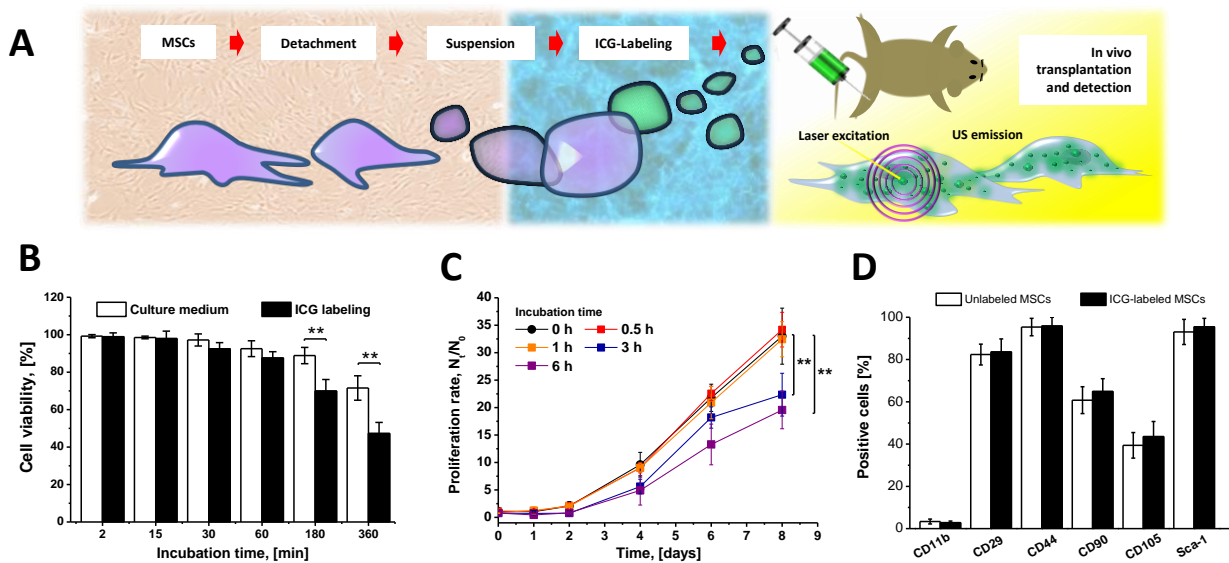40. J. V. Frangioni and R. J. Hajjar, Circulation **110**, 3378-3383 (2004).

Figures

Figure 1. Cytotoxic effects induced by the ICG. (**A**) Schematic diagram of the adopted procedure for ICG-labeling and *in vivo* detection of MSCs. (**B**) Cell viability estimated on MSCs incubated with 0.25 mg/ml ICG-containing medium for different time ranges. Cells incubated with culture medium were used as control. (**C**) Proliferation rate of MSCs subjected to the ICG-labeling for different time ranges (0 h refers to control cells that did not undergo the labeling procedure). (**D**) Marker expression profiles analysed by flow cytometry showing a high conformity between ICG-labeled and unlabeled MSCs. A basic characterization of the primary murine stem cells was provided through the analysis of different surface markers defining the MSC profile (CD44^{+}, CD90^{+}, CD29^{+}, CD105^{+}, Sca-1^{+}, and CD11b^{-}).
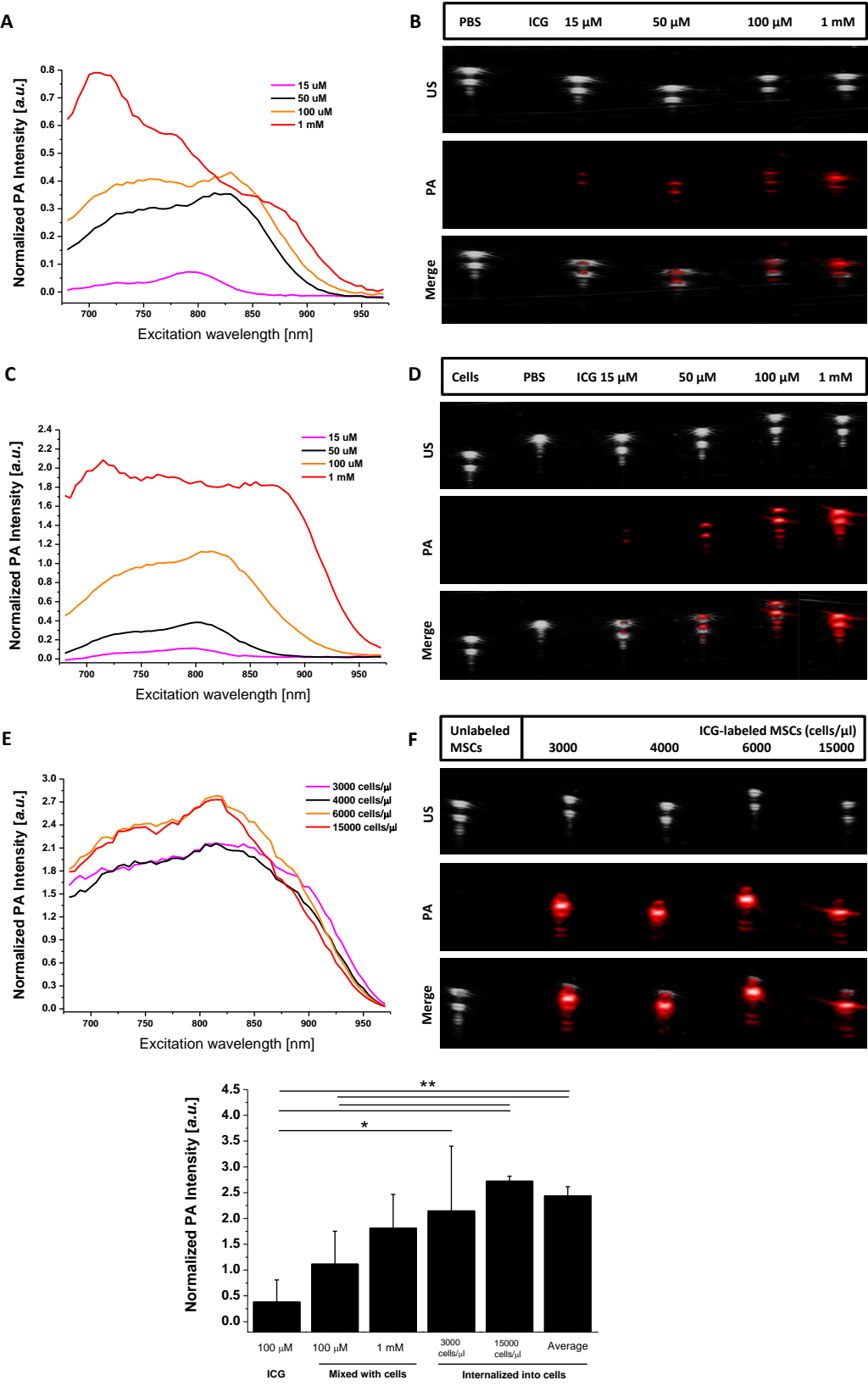
Figure 2. In vitro PA imaging of ICG. Photoacoustic spectra (**A, C,** and **E**) and representative imaging (**B**, **D**, and **F**) in pure photoacoustic mode (PA), ultrasounds (US) or merged imaging of: aqueous ICG solutions at different concentrations (**A** and **B**), 3.0×10^5 unlabeled MSCs resuspended in differently concentrated ICG solutions (**C** and **D**) and 3.0×10^5 ICG-labeled MSCs resuspended at different cell concentrations in PBS (**E** and **F**). (**G**) PA signal quantification at fixed wavelength (810 nm) of ICG in free form, in the presence of cells, and internalized into cells after labeling. 'Average' refers to average value of signal from all cell densities conditions. Statistical significance was determined by the unpaired Student *t*-test.
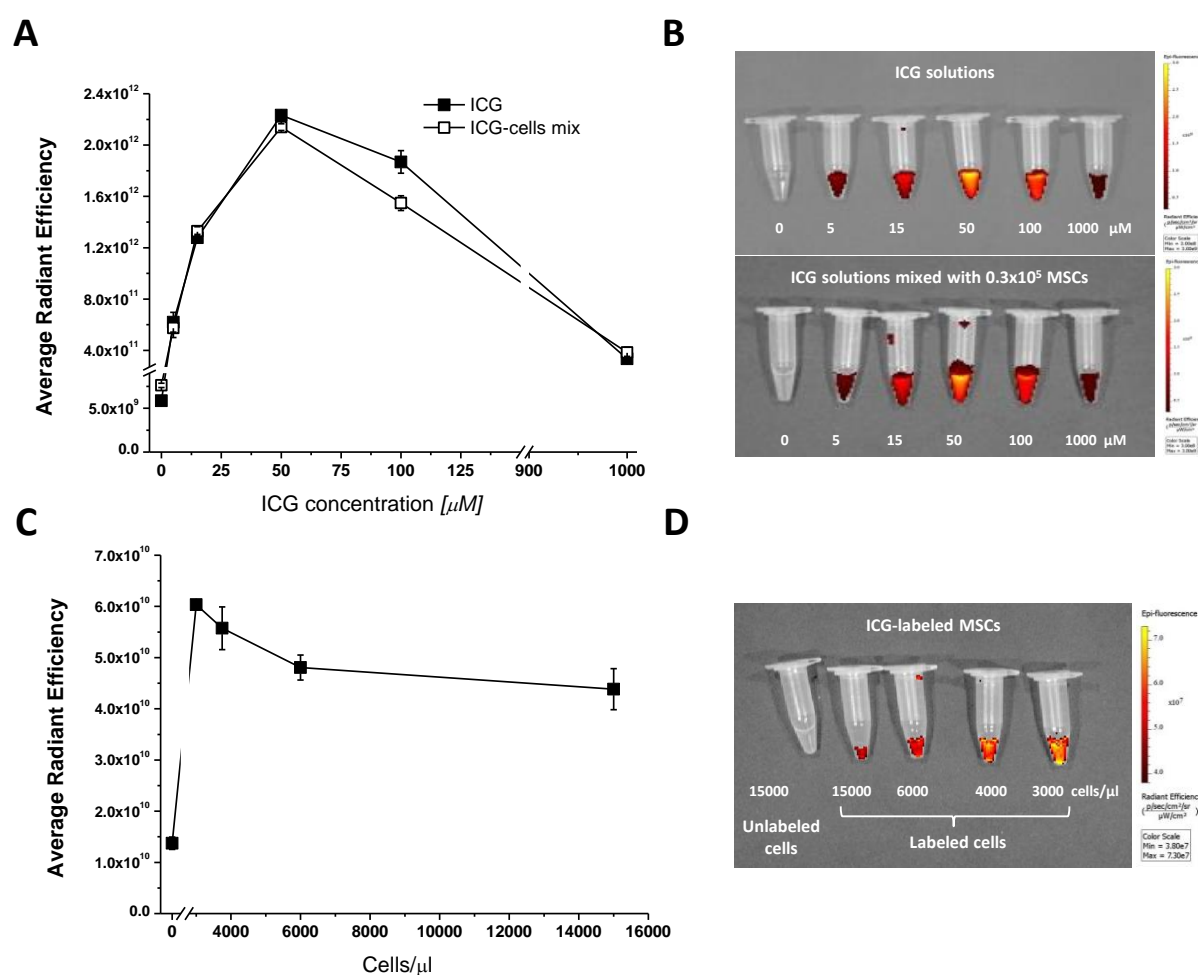
A

B

C

D

Figure 3. In vitro optical imaging of ICG. Fluorescence intensity (as expressed in average radiant efficiency) and representative imaging of aqueous ICG solutions at different concentrations either in the absence or in the presence of 3.0×10^5 unlabeled MSCs (**A** and **B**), and differently concentrated suspensions of ICG-labeled MSCs (**C** and **D**).
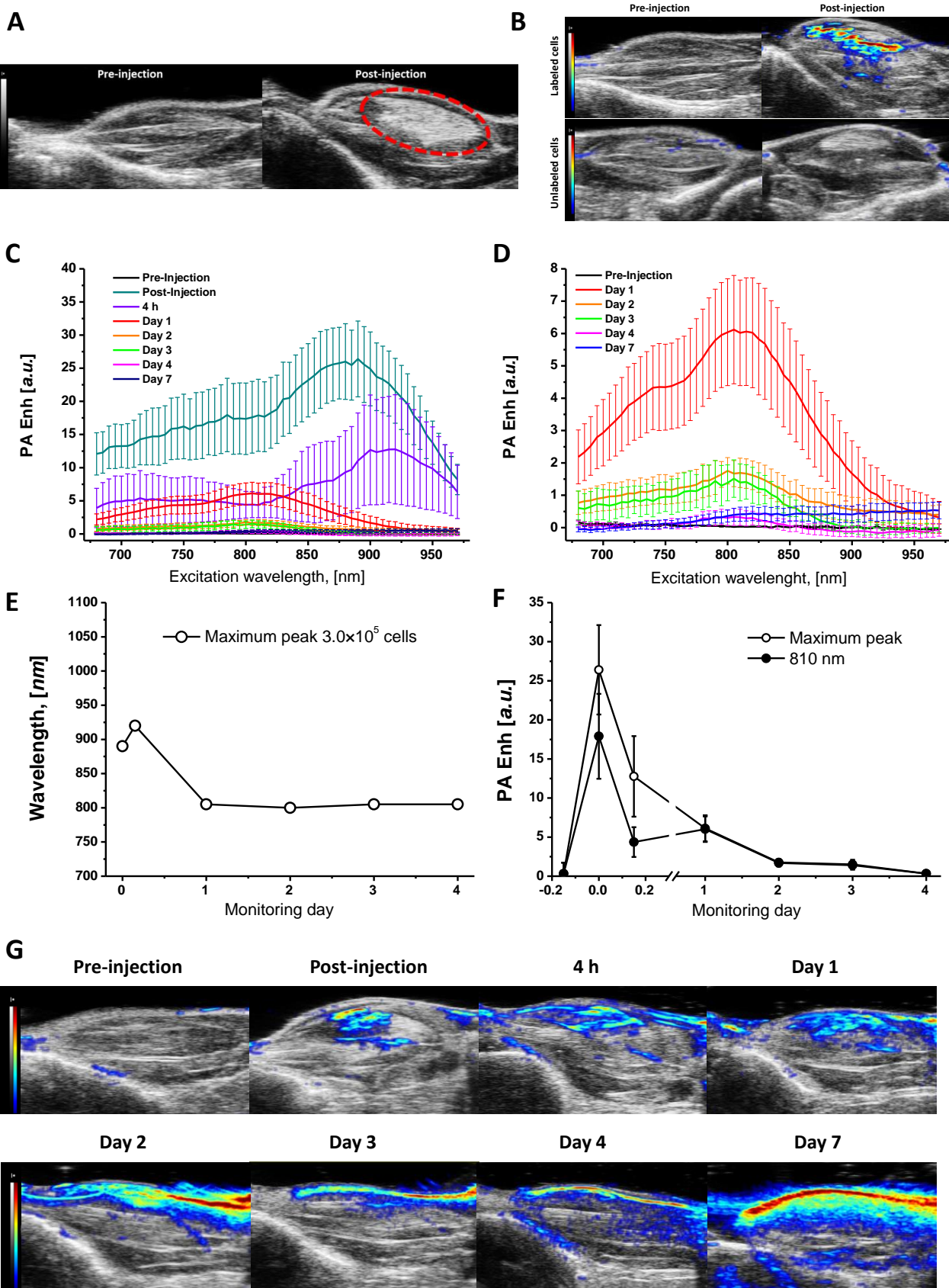
Figure 4. *In vivo* **local PA Signal Intensity after cell transplantation.** (**A**) Representative B-Mode Ultrasound imaging showing the deposition site of 3.0×10^5 unlabeled MSCs after intramuscular transplantation. (**B**) Representative combined Ultrasound and Photoacoustic (US/PA) images recorded at the PA excitation wavelength of 810 nm, showing the inoculation site before and after the transplantation of 3.0×10^5 ICG-labeled MSCs (right hindlimb, top), or an equivalent number of control unlabeled cells (left hindlimb, bottom). (**C**) Photoacoustic spectra recorded in the inoculation site at variable time ranges after cell deposition, expressed as Photoacoustic enhancement (PA Enh) over the control unlabelled cells. (**D**) Shape of the photoacoustic spectra recorded at time points starting from day 1. (**E**) Excitation wavelength of the main peak in the PA spectra during monitoring. (**F**) Photoacoustic contrast enhancement measured at the excitation wavelength of 810 nm and at that corresponding to the maximum spectral peak. (**G**) Representative PA monitoring (fixed excitation wavelength: 810 nm) of the cell engraftment over days. ROIs were drawn on the muscular region (internal area of the hindlimb), excluding the unspecific signal generated by the skin-induced reflection artefacts (tissue depth $\leq$ 1mm).
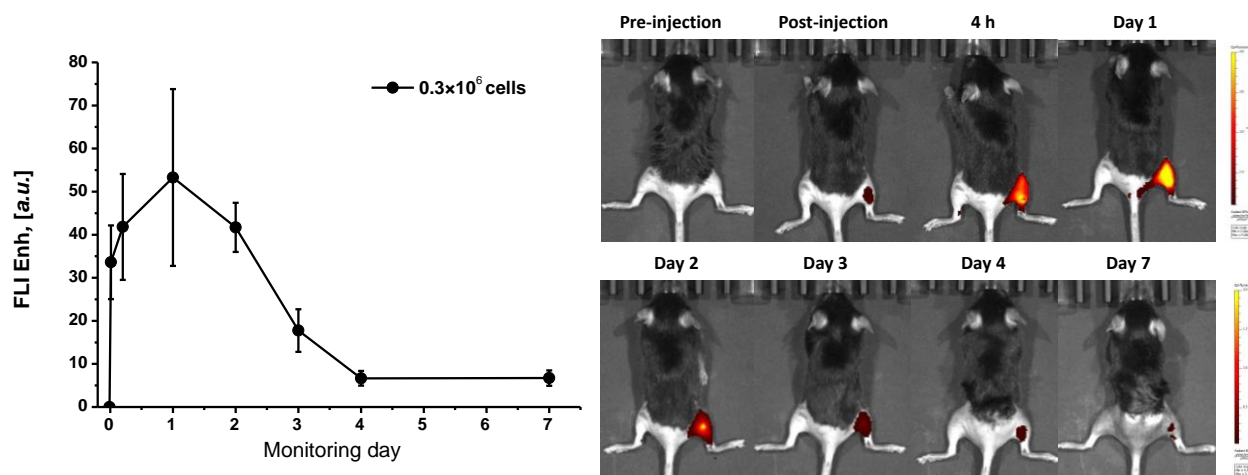

Figure 5. *In vivo* **optical imaging.** Fluorescence signal intensity measured after the transplantation of 3.0×10^5 ICG-labeled MSCs (excitation and emission wavelengths: 745 and 840 nm, respectively) and expressed as Fluorescence Imaging Enhancement (FLI Enh) over the control unlabeled cells **(A)**. Representative optical images showing the time persistence of the fluorescent signal after the cell transplantation (color scale: 2.0×10^8-4.0×10^9 for images in the top row, 4.0×10^7-2.0×10^9 for images in the bottom row) **(B)**. Calibration bars are shown.

Graphical Abstract
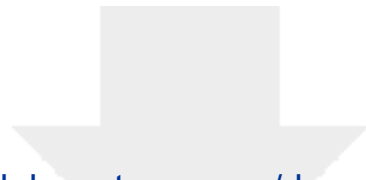
Click here to access/download
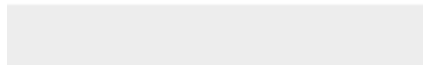Supporting Information
Graphical Abstract for Table of Contents.docx
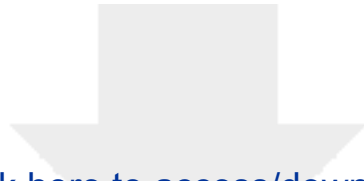
Click here to access/download
Supporting Information
Supplementary info_ICGlabeling.docx

Click here to access/download
Supporting Information
Movies.zip

Click here to access/download
Supporting Information
CV and photo of authors.docx